PAPER • **OPEN ACCESS**

Pinning properties of Y211 added cold top-seeded YBCO grown on Y_2O_3 layer

To cite this article: Bakiye Çakr *et al* 2016 *J. Phys.: Conf. Ser.* **707** 012034

Pinning properties of Y211 added cold top-seeded YBCO grown on Y_2O_3 layer

Bakiye Çakır[1,2], Şeyda Duman[3], Alev Aydıner[1]

[1]Department of Physics, Faculty of Sciences, Karadeniz Technical University, Trabzon 61080, Turkey,
[2]Department of Elementary Education, Faculty of Education, Artvin Çoruh University, Artvin 08000, Turkey
[3] Vocational School of Health Services, Artvin Çoruh University, Artvin 08000, Turkey

E-Mail: bakiye.cakir@gmail.com

Abstract. In this study, samples having different composition were prepared with the cold top seeding-melt-growth (TSMG) process by using Nd123 seed. Y_2O_3 buffer layer was placed to bottom of the pellets consist of Y123: Y211 powder mixtures. Two samples were fabricated in stoichiometric ratios of 1:0 and 1:0.4 labeled as Y0 and Y40, respectively. The T_c onset values of Y0 and Y40 were found to be 93.4 and 93.6 K at 0 T, respectively. The dependence of the effective activation energy U of the flux pinning on the magnetic field and temperature of the sample were determined using the Arrhenius activation energy law from the resistivity curves. The magnetization measurements were performed using a vibrating sample magnetometer (VSM) at 30, 50 and 77 K. The critical current densities (J_c) for Y0 and Y40 samples were determined to be 5.1×10^3 and 3.7×10^3 A/cm^2 at 77 K in 0 T, respectively. The normalized pinning force density versus the reduced field was examined at different temperatures to determine the pinning mechanism.

1. Introduction

Superconducting $YBa_2Cu_3O_{7-x}$ (Y123) bulks grown by TSMG method is a promising candidate for high performance superconducting samples. This is mainly due to their abilities of trapping magnetic flux and high critical current density (J_c), which allows practical applications such as permanent magnets, magnetic levitation, magnetic bearings, and flywheels. Because, for practical applications high temperature superconductors (HTS) need to carry a high critical current density under high magnetic fields. On the other hand, the supercurrent of YBCO bulk is limited by the weak links and flux creep, which is caused by grain boundaries and thermal activation, respectively [1].

On the other hand, it is well established that the presence of non-superconducting second phase Y211 particles of sizes ~1 μm embedded in the superconducting Y123 phase matrix correlates with enhanced flux pinning in YBCO. Reducing the size of these particles, ideally to dimensions of the order of double the coherence length of the system, increases their magnetic flux pinning potential further [2,3].

The unusual small coherence length leads to an unusual low pinning energy. However, due to vortex motion, the capability of YBCO to carry currents is significantly reduced at high value of the applied magnetic fields. To understand the complex pinning behavior in HTS, an important aspect is to study the dependence of the effective activation energy U of the flux pinning on the magnetic field and temperature. One accepted method for probing this dependence is to measure the resistive transition in various applied magnetic fields and temperatures. It is commonly suggested that the resistivity of HTS in the region of low resistivity can be described by the Arrhenius equations [4].

There have been a lot of interests in understanding the mechanism of pinning in YBCO based superconducting nanocomposites. The non-superconducting nanoparticles such as Y211 particles trapped in YBCO superconducting matrix can act as effective pinning centers leading to enhanced

critical current density. However, Y_2O_3 layer was used to absorb the unreacted Y211 liquid phase during the crystal growth process.

The critical current density J_c at an induction B is that which allows the Lorentz force to be just balanced by a flux pinning force (F_p). The flux-line lattice in mixed state is assumed to be pinned by the interaction with pinning centers, which are the features of the microstructure of the superconductors [5]. Hence, it is very important to correctly understand the flux pinning mechanism. Flux pinning in superconductors may be caused by spatial fluctuations of the transition temperature T_c ("δT_c–pinning") or of the charge carrier mean free path ("δl–pinning") near a lattice defect [6]. δl pinning centers behave like normal conducting particles and are very effective to provide pinning at low fields and low temperatures. However, δT_c pinning centers behave like the local oxygen deficient regions and are only effective at the intermediate fields and temperatures [7].

In this study, due to the use of Y_2O_3 nanoparticles showed a potential as flux-pinning centers in YBCO thin films and the layer was effective on crystal growth mechanism for bulk YBCO [8], a TSMG YBCO sample was grown on the Y_2O_3 layer with Y211 addition and without any addition. Also, activation energies and the dominant flux pinning mechanism of strong pinning centers of the samples were investigated to obtain effect of the Y211 addition and Y_2O_3 layer.

2. Material and methods

YBCO bulk samples with nominal composition $YBa_2Cu_3O_{7-x}$ (Y123) with $YBaCuO_5$ (Y211) addition were fabricated by TSMG process by using Nd123 seed. The starting Y_2O_3, $BaCO_3$, and CuO powders were mixed with a molar ratio 1:2:3 to synthesize Y123 composition, which was then calcined within a box furnace at 900°C for 24h. The calcination process was performed three times with intermediate grindings for 15 minutes. The Y211 composition was made in a similar way to Y123, but ground for 45 minutes. After the calcination process the fine Y123 powders were then placed into a platinum crucible and put into the muffle furnace at room temperature. The furnace temperature was increased to 1450°C and held at that temperature for 5 min. to get molten material. The molten material was then poured onto a cupper plate, and afterwards sandwiched with another cupper plate to protect phase condition during melt. The obtained thin platelets were ground again for 15 min. to achieve fine powder. These Y123 powders were then mixed with Y211 powders in molar ratio Y123:Y211 = 1:0 and 1:0.4 and fabricated samples were labeled as Y0 and Y40, respectively. The mixed precursor powder was pressed into a pellet of diameter 20 mm and height 8 mm. An Nd123 seed was centrally placed on top of the pellet. Crystal growth process was performed on an alumina crucible with Y_2O_3 layer as heat treatment was applied as shown in Figure 1. Finally, the grown sample were annealed at 500 °C for 200 h in flowing oxygen and then cooled to room temperature at a rate of 1 °C.min^{-1} in oxygen.

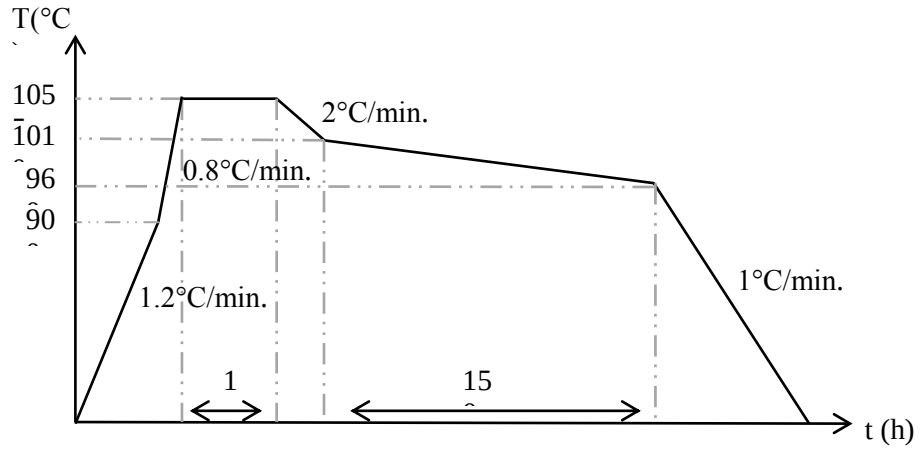

Figure 1. Schematic diagram of thermal process for YBCO samples

For determining characteristic peaks of Y123 sample was obtained after crystal growth, X-ray diffraction data were collected by using a Rikagu D/Max III C diffractometer, employing CuKα (λ = 1.5418 Å, 40 kV, 30 mA) radiation. 2θ range 20 to 60° was scanned in steps of 0.02° in the atmosphere with a counting time 3°/min.

Resistivity measurements were performed by a standard four-probe method at temperatures between 40 and 120 K at a rate of 4 $Kmin^{-1}$ using a Quantum Design physical properties measurement system (PPMS) under various constant magnetic fields from 1 to 5 T with the magnetic field parallel to the *c*-axis, which is the direction of pressing into the zero-field cooling regime (ZFC). Having completed the measurement at a given magnetic field for each cycle, the field was set to zero, and the temperature was increased to 120 K to completely remove the trapped field inside the sample. Effective activation energy *U* of the flux pinning on the magnetic field and temperature of the sample were determined from the resistivity curves.

The magnetization properties were measured using a vibrating sample magnetometer (VSM) for the respective constant temperatures such as 30, 50, and 77 K with the magnetic field parallel to the *c*-axis, which is the direction of compaction. The M-H measurements were performed using the sweep rate of 100 mTs^{-1}. All the magnetization measurements were done in the ZFC regime. After completing the measurement at a given temperature for an each cycle, the field was set to zero and the temperature was warmed to 120 K to completely remove the trapped field inside the sample. The critical current density, J_c (A/cm^2), was calculated from the magnetization hysteresis loops based on the extended Bean model [9]. The normalized pinning force density (f_p) derived from the J_c versus the reduced field (*b*) was examined at different temperatures to determine the pinning mechanism.

3. Results and discussion

X-ray diffraction pattern of the Y0 and Y40 could be seen in Figure 2. It was observed in Figure 2(a) that only a dominant characteristic superconducting (103) peak was seen for Y0, indicating highly superconducting structure.

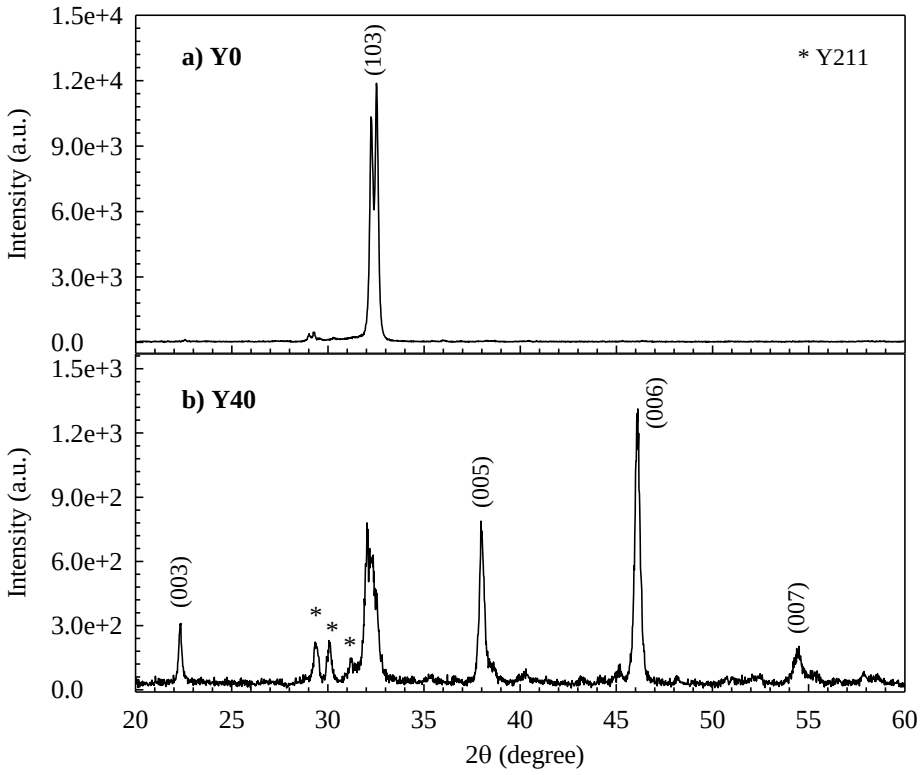

Figure 2. X-ray diffraction patterns of the a) Y0 and b) Y40 samples.

At the same time, there are small peaks of the Y211 phases revealing the presence of the Y211 particles in the sample and characteristic superconducting (103) peak in the spectrum at around $2\theta \sim 32.5°$ for Y40 as shown in Figure 2(b). Moreover the (00*l*) peaks were clearly observed, representing that these specimens are highly oriented by the *c*-axis perpendicular to the top surface. It was known that if the seed does not dissolve, this leads to the formation of the single-domain structure [10]. Although, both two samples were fabricated under the same condition, the samples had different XRD pattern. It was known that geometrical shape and single crystal structure of the seed are important parameters for fabrication of the bulk single crystal rather than the thermal process [11].

Figure 3 shows the normalized resistive superconducting transitions up to 5 T as a function of temperature for the Y0 and Y40 samples. Table 1 lists the onset point ($T_{c,onset}$), zero point ($T_{c,zero}$) and superconducting transition width□(□T) of the samples estimated in the resistivity–temperature plots taken under different applied magnetic fields. Additionally, sharp superconducting transition were achieved for Y0 and Y40 samples and the $T_{c,onset}$ values obtained to be 93.4 and 93.6 K at 0 T, respectively. Also, it can be observed that the zero resistance temperature decreases with further increase of the magnetic field. However, the magnetic dispersion of Y40 was very little, indicating the strength of the sample against the applied magnetic field. For the samples, it was seen that the superconducting transitions was quite small compared with other results [4, 12]. The large □T values imply very sluggish oxygen diffusion into the large sized single Y123 grains in spite of the presence of the Y211/Y123 interfaces [13].

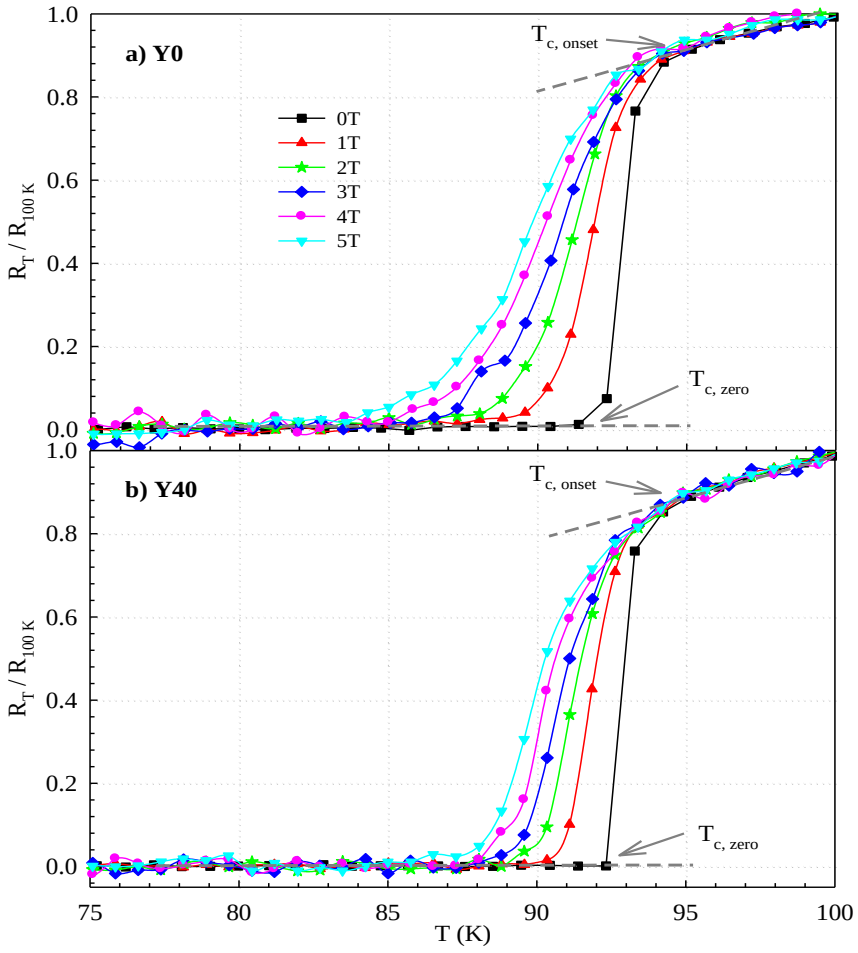

Figure 3. Normalized resistive superconducting transitions as a function of temperature for the a) Y0 and b) Y40 samples at different applied field.

Table 1. The values of critical transition temperatures for the sample Y0 and Y40 under different magnetic fields.

			0T	1T	2T	3T	4T	5T
Y0	$T_{c,onset}$	(K)	93.4	93.1	92.8	92.6	92.4	91.9
	$T_{c,zero}$	(K)	92.2	90.5	89.4	87.9	87.2	85.4
	ΔT	(K)	1.2	2.6	3.4	4.7	5.2	6.6
Y40	$T_{c,onset}$	(K)	93.6	92.6	92.6	92.3	92.1	91.9
	$T_{c,zero}$	(K)	91.9	89.9	89.0	88.1	87.8	87.3
	ΔT	(K)	1.7	2.8	3.6	4.2	4.3	4.6

When the Lorentz force per unit volume exceeds the pinning force per unit volume (F_p), electrical resistance is introduced because of flux flow. It is well established that lowering the temperature increases both the pinning strength and the pinning force. However, at high temperatures, the effect of pinning strength is suppressed by thermal fluctuations [14]. Because of the thermally activated flux flow (TAFF) of vortices, the resistive transition suppressed to lower temperature with the increase of applied magnetic field and it can be well described by Arrhenius dependence [15]

$$\rho(B,T) = \rho_0 \exp[-U(B,T)/k_B T] \tag{1}$$

where U (B,T) is activation energy for flux creep that depends on the temperature and magnetic field, ρ (B,T) is resistivity in a magnetic field, ρ_0 is maximum resistivity, T is temperature and k_B is the Boltzmann constant. For the case of classical flux creep [16], where $U >> k_B T$, the activation energy should not depend on temperature. According to the Eq. 2, the activation energy (U) value can be directly deduced from the slope of the plot of ln (ρ/ρ_0) versus $1/T$.

$$U = -k_B T \ln[\rho/\rho_0] \tag{2}$$

Figure 4 illustrates the plots of ln (ρ/ρ_0) versus $1/T$ of the Y0 and Y40 samples under different external magnetic fields from 0 to 5T and insets the plots of U versus magnetic fields. As one can see for each curve the activation energy decreases with the increase of the applied magnetic field. However, the activation energies observed for the sample Y0 and Y40 in applied magnetic fields were 0.69 and 1.78 in zero magnetic field, 0.13 and 0.28 *eV* in 5 *T* magnetic field, respectively. Also, the activation energies of the Y40 were higher than the Y0 because of flux pinned by the Y211particles acting as pinning centers in Y40 is shown in insets plot of the Figure 4. The calculated values of the activation energies for Y0 and Y40 showed significantly higher than the values reported in literature for BSCCO and YBCO bulk produced by solid state reaction method [17–20]. Decrease of the activation energy depending on the increasing magnetic field causes vortex motion easily. That is, it can be said that the number of pinning centers are reduced and the superconducting properties are declined with the increasing magnetic field.

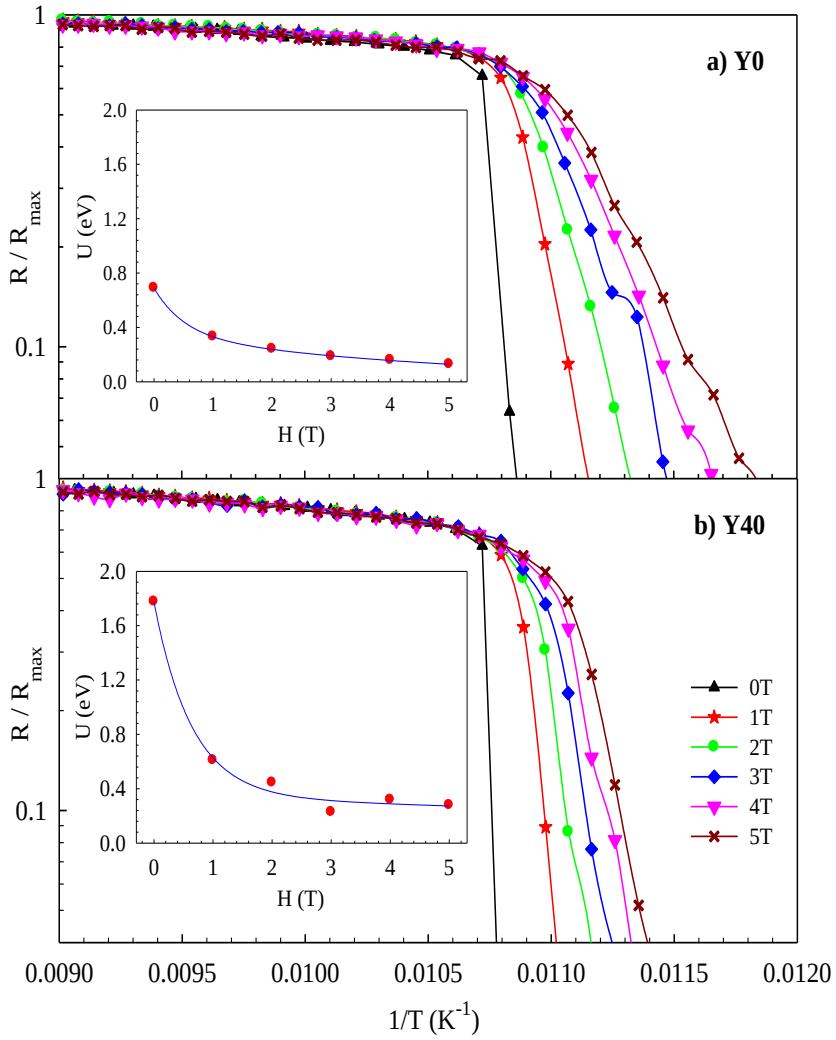

Figure 4. Resistive transitions as a function of temperature in semi-logarithmic scale and dependence of the activation energy on the magnetic field (*inset*) for a) Y0 and b) Y40 samples.

Figure 5 shows the variation of critical current density by the applied magnetic field for Y0 and Y40 samples at 30, 50 and 77 K. Critical current density (J_c) was calculated from the magnetization hysteresis based on the critical state model [9]. The J_c values for Y0 and Y40 samples were determined to be 5.1×10^3 and 3.7×10^3 A/cm^2 at 77 K in 0 T, respectively and could be seen in Table 2 at different temperatures under magnetic field from 0 to 5T. Although any Y211 addition was not used for Y0, there was no explicit difference in terms of order between critical current densities for the samples, because, the Y_2O_3 layer prevent the losing of the liquid phase. However, J_c of the Y0 samples higher than the Y40 at the lower temperatures in contrast to 77 K. In the low field and high temperature region, J_c decreases sharply with temperature, which was attributed to the flux pinning created by the linear correlated disorders between Y211 and Y123 grains [21]. It is clearly seen from the figures that the J_c varies almost linearly with the increasing magnetic field. This variation indicates that the samples are strong enough against a magnetic field. It is established that the Y211 particles are the source of strong pinning. It is also known that the linear behavior of J_c, attributes to the low values of flux creeps in samples.

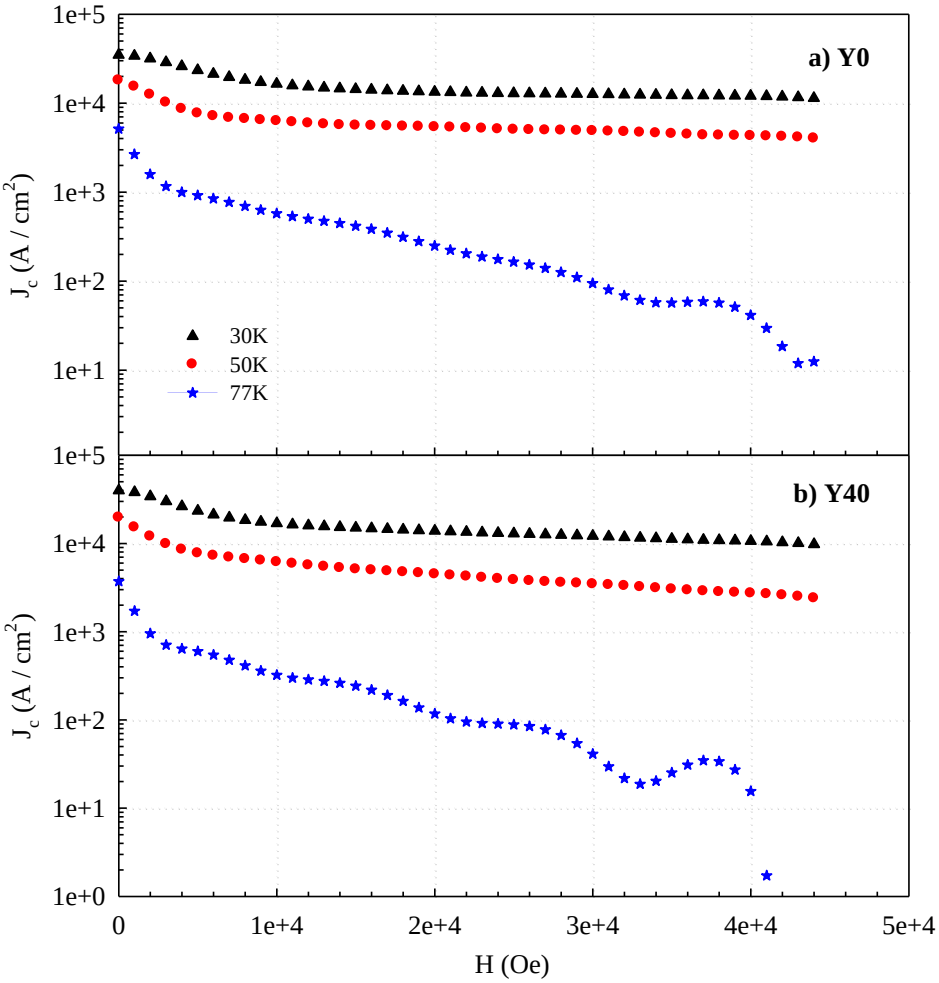

Figure 5. Critical current density as a function of the magnetic field at different temperatures for the a) Y0 and b) Y40.

Table 2. The values of critical current densities for the samples Y0 and Y40 under different magnetic fields.

		0 T	**1 T**	**2 T**	**3 T**	**4 T**
Y0	J_c (A/cm^2) (30 K)	3.48×10^4	1.64×10^4	1.34×10^4	1.26×10^4	1.21×10^4
	J_c (A/cm^2) (50 K)	1.80×10^4	0.63×10^4	0.54×10^4	0.48×10^4	0.43×10^4
	J_c (A/cm^2) (77 K)	5.13×10^3	5.73×10^2	2.48×10^2	0.94×10^2	0.41×10^2
Y40	J_c (A/cm^2) (30 K)	3.98×10^4	1.69×10^4	1.39×10^4	1.21×10^4	1.06×10^4
	J_c (A/cm^2) (50 K)	1.96×10^4	0.61×10^4	0.45×10^4	0.34×10^4	0.27×10^4
	J_c (A/cm^2) (77 K)	3.71×10^3	3.21×10^2	1.17×10^2	0.41×10^2	0.16×10^2

In order to give an explicit insight into the pinning mechanism an extended analysis of scaling laws was investigated because of the importance of the flux pinning force (F_p). According to the Dew-Hughes model [5], the F_p can be written as follows;

$$F_p(b) = Ab^m(1-b)^n \quad (3)$$

where, $b = B/B_{\max}$, A is a constant and *m*, *n* are parameters which is rely on the defect geometry (pointlike, linear, planar or surface, etc.), the type of interaction (core or magnetic) and the type of pinning center (normal or superconductor having different properties with respect to the bulk) that depend on the flux pinning mechanism. In order to obtain a deeper insight into the origin of the improved pinning properties, an extended analysis of the volume pinning force $F_p = J_c B$ is examined. Actually, in the high-temperature superconductors, $f_p(b) = F_p / F_{\max}$ often scales with $b = B/B_{irr}$ but it is quite difficult to determine the correct B_{irr} values using the DC magnetic measurement and several authors succeeded in scaling indicated that B_{max} exhibits an identical temperature dependence with that of B_{irr} and that B_{max} can be used as a scaling field where B_{max} is the field at which F_p exhibits a maximum at $B = B_{max}$ [22, 23].

The scaling of $f_p - b$ for high–T_c superconductors is often analyzed using the following Eq. 4(a–c) [22–24]:

$\Delta\kappa$ pinning	$f_p(b) = 3b^2(1-2b/3)$	(4a)
Normal point pinning	$f_p(b) = (9b/4)(1-b/3)^2$	(4b)
Surface pinning	$f_p(b) = (25\sqrt{b}/16)(1-b/5)^2$	(4c)

The normalized pinning force density $f_p(b) = F_p / F_{p\max}$ versus reduced field $b = B/B_{\max}$ are plotted in Figure 6, for the Y0 and Y40 samples at 30, 50 and 77K. Also Eq. 4(a–c) is represented in this figure to determine the pinning mechanism. At 30 K, the experimental results were appropriate for normal point pinning mechanism in a low field region (b < 0.2), the results are changed between $\Delta\kappa$ pinning and normal point pinning for both samples when b < 0.7 and b close to 1 then $\Delta\kappa$ pinning was good agreement for both samples. At 50 K, in low fields, normal point pinning was dominant for Y40 due to addition of the Y211 particles while the results for the Y0 between $\Delta\kappa$ pinning and normal point pinning. It has been proved that relatively large Y211 particles contribute to flux pinning in Y123 superconductors [25]. Y211 particles in Y123 superconductors have the proportionality of $F_p \propto N_p D^2$ where N_p is number of the Y211 inclusions per unit volume and *D* their mean diameter. Also, contribution of the $\Delta\kappa$ pinning mechanism may be operating is the local variations in T_c due to substitutions, doping, oxygen vacancy clusters [25, 26]. The normalized pinning force density results at 77 K disagree with a certain pinning mechanism (Figure 6(c)). The samples were convenient with surface pinning higher than the B_{max} the mechanism was changed between $\Delta\kappa$ pinning and normal point pinning for b < 0.5 and the mechanism was varied between normal point pinning and surface pinning for b > 2.5. So, it was thought that there was some another contribution coming from the other magnetic interactions such as ferromagnetism or anti-ferromagnetism. Pinning performance for the samples in a low field region is closely related with the dispersion of non-superconducting particles, whose average diameter is larger than the coherence length ξ [23].

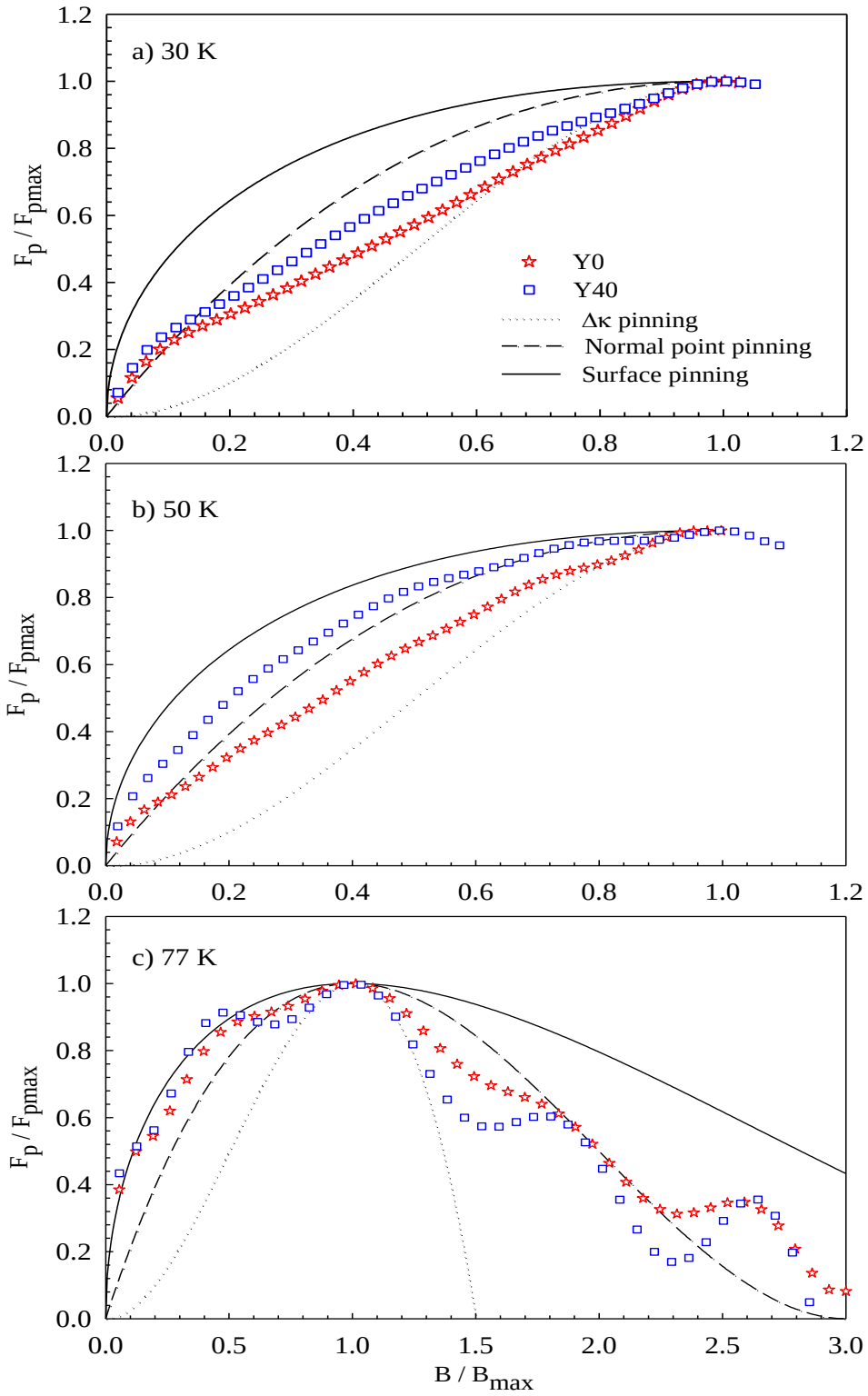

Figure 6. The normalized pinning force density $f_p(b)$ versus reduced field b are plotted for the Y0 and Y40 samples at a) 30K, b) 50K and c) 77K.

4. Conclusion

Two samples were fabricated by TSMG methods with Y_2O_3 layer in stoichiometric ratios of Y123: Y211 as 1:0 and 1:0.4 named as Y0 and Y40, respectively. Results of the physical properties and pinning mechanism of the samples are shown in below;

1. The magnetic dispersion of Y40 was very little indicating strength of the sample against the applied magnetic field.
2. The activation energies of the Y40 were decreased more rapidly when it compared to the sample Y0. Because population of the non-superconducting Y211 particle of the Y40 sample was higher than the Y0 at low magnetic field flux pinned by the Y211 particles acting as pinning centers.
3. Although any Y211 addition was not used for Y0, there was no explicit difference between the critical current densities for the samples in terms of order. Because, Y_2O_3 layer prevent the losing of the liquid phase. However, J_c of the Y0 samples higher than the Y40 at the lower temperatures in contrast to 77 K.
4. Both samples had almost same pinning behavior and normal cores type pinning and $\Delta\kappa$ pinning was observed dominantly at different temperatures. Although any Y211 adding did not used for Y0 pinning behavior not changed, because Y_2O_3 layer supports the Y211 phase during the crystal growth process. It was thought that the pinning is due to Y211 particles in low fields.

References

[1] Li J, Yang W, Wang M, Guo Y and Feng Z 2015 *J Supercond. Nov. Magn.* 28 1725-1728.
[2] Hari Babu N, Reddy E S, Cardwell D A, Campbell A M, Tarrant C D and Schneider K R 2003 *Appl. Phys. Lett.* 83 23.
[3] Moutalbi N, Ouerghi A, Djurado E, Noudem J G and M'chirgui A 2011 *Physica C* 471, 97-103
[4] Zou X W, Wang Z H, Chen J L and Zhang H 2001 *Physica C* 356 31-38.
[5] Dew-Huges D 1974 *Philos. Mag.* 30 2 293-305.
[6] Giller D, Shaulov A and Yeshurun Y 2000 *Physica B* 288 687-688.
[7] Kim G C, Kim B J, Cheon M Y and Kim Y C 2003 *Physica C* 391 305-308.
[8] Çakır B and Aydıner A 2011 *J. Supercond. Nov. Magn.* 24 1577-1584.
[9] Ben Salem M K, Hannachi E, Slimani Y, Hamrita A, Zouaoui M, Bessais L, Ben Salem M and Ben Azzouz F 2014 *Ceramics International* 40 4953-4962.
[10] Cloots R, Koutzarova T, Mathieu J P and Ausloos M 2005 *Supercond. Sci. Technol.* 18 R9.
[11] Diko P, Zmorayova K, Babu N H and Cardwell D A, 2003 *Physica C* 398, 1-7.
[12] Liu S L 2008 *J. Supercond. Nov. Magn.* 21 199.
[13] Jun B-H, Jung S-A, Park S-D, Park B J, Han Y H and Kim C-J 2011 *Physica C* 471 876-879.
[14] Benkraouda M, Obaidat I M and Al Khawaja U 2006 *Physica C* 433 205-211.
[15] Anderson P W 1962 *Phys. Rev. Lett.* **9** 7 309-311.
[16] Balaev D A, Dubrovskiy A A, Popkov S I, Shaykhutdinov K A and Petrov M I 2008 *J. Supercond. Nov. Magn.* 21, 243.
[17] Balchev N, Nenkov K and Antonov V 2013 *J. Supercond. Nov. Magn.* 26 59-63.
[18] Çelik Ş, Öztürk K and Yanmaz E 2008 *J. Alloys and Compounds* 458 30-36.
[19] Kameli P, Salamati H, Abdolhosseini I and Sohrabi D 2008 *Physica C* 468 137-141.
[20] Kutuk S, Bolat S, Terzioğlu C and Altintas S P 2015 *J. Alloys and Compounds* 650 159-164.
[21] Okram G S, Aokia H and Nakamura K 1999 *Solid State Commun.* 110 327-331.
[22] Higuchi T, Yoo S I and Murakami M 1999 *Phys. Rev. B* 59 1514-1527.
[23] Goto T, Inagaki K and Watanabe K 2000 *Physica C* 330 51-57.
[24] Taylan Koparan E, Surdu A, Sidorenko A and Yanmaz E 2012 *Physica C* 473 1-5.
[25] Zablotskii V, Jirsa M and Petrenko P 2002 *Phys. Rev. B* 65 2245081.
[26] Koblischka M R, Muralidhar M and Murakami M 2000 *Physica C* 337 31-38.